OPEN ACCESS
IOP Publishing
Measurement Science and Technology
Meas. Sci. Technol. **34** (2023) 125013 (12pp)
https://doi.org/10.1088/1361-6501/acf061

Thermal induced deflection in atomic force microscopy cantilevers: analysis & solution

Christopher W Mordue*, Jonathan M R Weaver and Phillip S Dobson

James Watt School of Engineering, University of Glasgow, Glasgow, United Kingdom

E-mail: christopher.mordue@glasgow.ac.uk

Received 3 May 2023, revised 17 July 2023
Accepted for publication 15 August 2023
Published 25 August 2023

Abstract

Atomic force microscopy (AFM) cantilevers are commonly made from two material layers: a reflective coating and structural substrate. Although effective, this can result in thermally induced cantilever deflection due to ambient and local temperature changes. While this has been previously documented, key aspects of this common phenomenon have been overlooked. This work explores the impact of thermally induced cantilever deflection when in- and out-of-contact, including the topographic scan artefacts produced. Scanning thermal microscopy probes were employed to provide direct cantilever temperature measurement from Peltier and microheater sources, whilst permitting cantilever deflection to be simultaneously monitored. Optical lever-based measurements of thermal deflection in the AFM were found to vary by up to 250% depending on the reflected laser spot location on the cantilever. This highlights AFM's inherent inability to correctly measure and account for thermal induced cantilever deflection in its feedback system. This is particularly problematic when scanning a tip in-contact with the surface, when probe behaviour is closer mechanically to that of a bridge than a cantilever regarding thermal bending. In this case, measurements of cantilever deflection and inferred surface topography contained significant artefacts and varied from negative to positive for different optical lever laser locations on the cantilevers. These topographic errors were measured to be up to 600 nm for a small temperature change of 2 K. However, all cantilevers measured showed a point of consistent, complete thermal deflection insensitivity 55% to 60% along their lengths. Positioning the reflected laser at this location, AFM scans exhibited improvements of up-to 97% in thermal topographic artefacts relative to other laser positions.

Keywords: atomic force microscopy, thermal drift, artefacts, thermal bend, bimetallic effect, scanning thermal microscopy

(Some figures may appear in colour only in the online journal)

* Author to whom any correspondence should be addressed.

1. Introduction

Atomic force microscopy (AFM) is a technique capable of generating nano-metre resolution images of a large range of surfaces. This is achieved by employing a cantilever spring with a sharp tip that is raster scanned across the surface of interest [1]. Using this approach, images can be realised by measuring the cantilever's deflection and inferring the tip-sample interaction force. Typically, the tip-force is controlled using a feedback loop allowing the microscope to generate a map of surface topography. With such an instrument, there are a range of topographic imaging modes including contact, intermittent/tapping contact and non-contact that can exploit and investigate different tip-sample interaction regimes [2]. All of these modes employ continuous monitoring of the tip-sample mechanical interaction during a scan. In the vast majority of commercially available instruments, this measurement is obtained by monitoring deflection of the cantilever using an optical lever arrangement [3], also called the optical beam deflection method [4]. This simple method is highly effective, but can be significantly sensitive to influences unrelated to tip-force. Specifically, relative movement between the sample and the AFM cantilever tip causes distortions and other artefacts in the resultant images [5]. A well-established source of such motion arises from AFM instruments often operating in areas that experience significant spatial or temporal temperature variations which can exceed ± 1 K [6, 7]. Moreover, the AFM itself has been shown to induce notable temperature change with cantilevers experiencing up to 6 K greater temperature than the surroundings [8]. This is a problem as temperature changes are well known to cause mechanical drift of stages and cantilever bend, which result in topographic artefacts [9, 10]. A major contribution to this is the common use of reflective coatings (typically a metal such as aluminium or gold) that can be found on many AFM cantilevers. These coatings are often intended to maximise reflection of the laser spot focused on the cantilever and hence enable low-noise deflection measurement in the optical lever system. Their improved reflectivity enhances the photodetector signal-to-noise ratio [11] and reduce optical interference artefacts [12]. A disadvantage of such coatings is the mismatch in coefficients of linear thermal expansion (CTE) between the reflective coating and the cantilever base material (e.g. silicon or silicon nitride) resulting in cantilever bending and deflection when exposed to temperature change. This observation is corroborated by the large reductions in cantilever thermal-deflection observed if no reflective coating is present [13]. Beyond these standard AFM probes, thin metallic film coatings are required on specialist probes to enable advanced imaging modes. Examples include conductive AFM [14], Kelvin probe force microscopy [15], magnetic force microscopy [16] and scanning thermal microscopy (SThM) [17]. In these instances, omission of the cantilever coating is not an option and thermal bending is inevitable. Researchers have aimed to mitigate thermally induced deflections by employing a variety of approaches, including thermally compensated stages [18], scanning/processing techniques [19–22], structurally compensated/altered probes [23, 24], thermal equilibration [25] and minimising the extent of the reflective coating [9]. Despite a widespread appreciation of the problem, little focus has been given to analysing exactly how thermal bending of the probe cantilever is interpreted within the optical lever system and how this interference interacts with the force feedback loop of the AFM. A schematic of this system can be seen in figure 1.

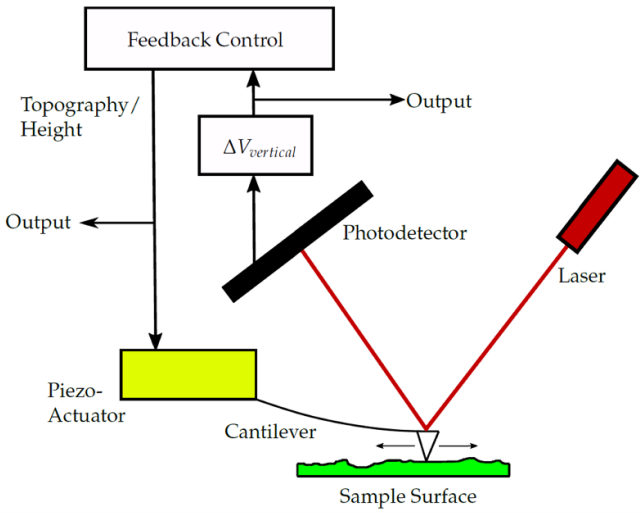

Figure 1. AFM simplified operation diagram.

In this work we have investigated this phenomenon for both out-of-contact and in-contact with a sample surface utilising KNT-SThM-1an/VITA–SThM probes (shortened henceforth to KNT-SThM) [26]. With a nominal spring constant and resonant frequency of 0.5 N m^{-1} and 50 kHz respectively, these employ electrical interrogation of a resistance thermometer located at their tip to measure its temperature. In order to minimise the connecting track's resistive contribution when measuring the tip resistor, these probes employ relatively thick (145 nm) gold (Au) wires that run the length of the cantilever, as shown in figure 2. Therefore, with this bimetallic propensity to thermally bend coupled with an ability to directly measure their tip temperature, they are an excellent tool to study thermal bending.

2. Key concepts

2.1. Optical lever & tip-deflection detection

As implemented in AFMs, the optical lever measures angular rotation or bending of the probe's cantilever by reflecting a laser off it onto a position sensitive photodetector [27], typically made up of a four quadrant photodiode. Displacement of this reflected laser spot on the four quadrants can then be related back to cantilever tip vertical and torsional deflections. This arrangement can be seen in figure 3 for vertical deflection.

One crucial aspect of this method that is often overlooked by many AFM users, is its direct measurement of cantilever rotation as opposed to tip vertical deflection. Rotation is converted to tip deflection, commonly called the inverse optical lever sensitivity (InvOLS), through the sample contact relation

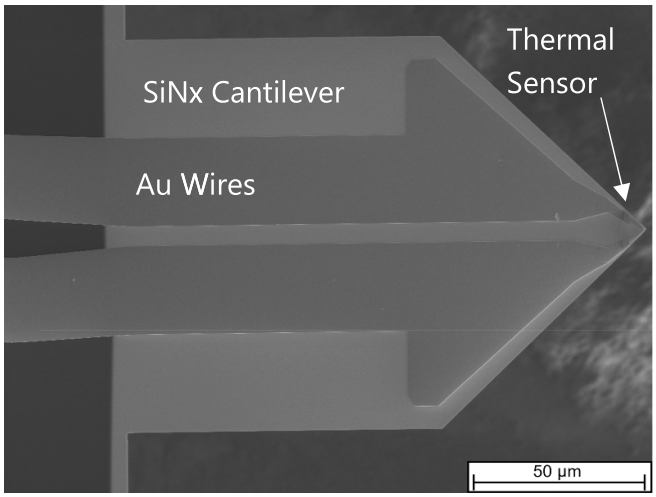

Figure 2. Scanning electron microscope image of a KNT-SThM cantilever.

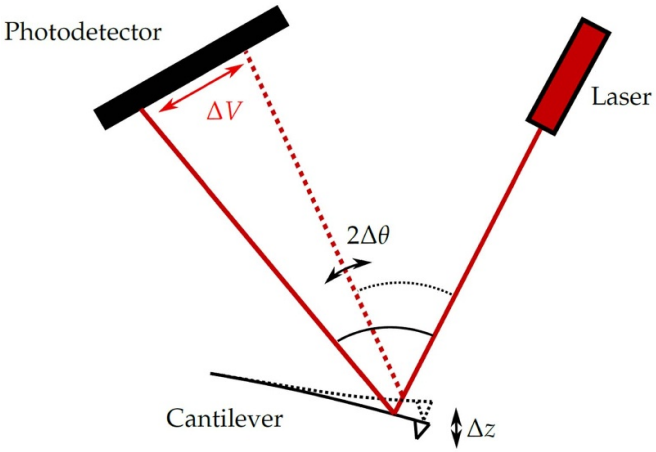

Figure 3. Simplified optical lever diagram within an AFM for vertical deflection.

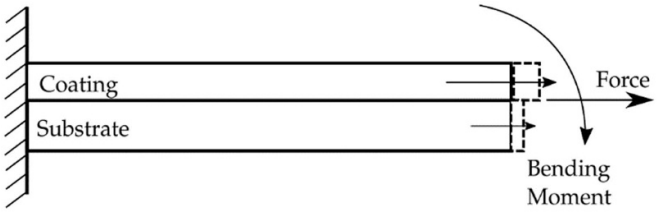

Figure 4. Thermal bending of a cantilever due to the bimetallic effect.

that induces tip-force [28]. This value is acquired by recording the photodetector's vertical output at the same time as deflecting the tip by a known distance [29]. However, the procedure must be repeated each time the probe or laser alignment is changed as these alterations will vary key parameters, such as the laser path length [4]. If the sensitivity calibration is performed correctly, the exact location of the reflected laser spot along the cantilever is theoretically inconsequential in determining tip deflection and subsequent force. Reflecting the laser from either the base or tip of the cantilever will output different photodetector signals, but will be converted to the same deflection thanks to the different InvOLS for each location. Despite this, there are practical reasons for positioning the laser spot nearer the tip as greater rotation occurs there, resulting in a larger photodetector signal for any given tip displacement and hence improved signal-to-noise performance [29]. This approach has long proven to be a reliable one, to the extent that many users may not even consider its underlying mechanisms. However, this stable relationship between rotation and tip deflection does not hold true for all sources of cantilever deflection, such as thermal bending.

2.2. Thermal bending of AFM cantilevers

The term thermal bending in AFM probes refers to the deflection of a cantilever due to changes in its temperature. This phenomenon has been documented by many authors [30, 31] who agree that its primary origin is the mismatched CTE possessed by the different layered cantilever materials. This mismatch in layer displacement and strain induced by temperature change causes different axial force magnitudes from each material. As the materials are strongly adhered to each other, this difference in axial force results in a bending moment from the material with greater CTE (which experiences greater displacement, strain and force) to the one with the lower CTE. This effect is frequently termed the 'bimetallic effect' [11], and is illustrated in figure 4. It is important to note that this type of cantilever deflection is fundamentally different to that produced by a tip-force in not only the source of deflection, but how it is generated along the cantilever length. Hence, for an identical tip deflection, the magnitude of rotations and deflections along the cantilever's length differs between a tip-force and thermally induced deflection. As a result, the AFM's InvOLS calibration using a tip-force cannot be used to accurately quantify thermal bending.

3. Measuring out-of-contact thermal bending

With the above understanding, KNT-SThM probes were employed to study AFM cantilever thermal bending since, as mentioned above, they provide an accurate measurement of tip temperature, permitting a direct link to be made between thermal and mechanical changes. This was achieved by systematically measuring deflections along the probe length for a given measured temperature change.

3.1. Optical profilometer profile

White light interferometry (Bruker, 3D Optical Profilometer, Contour GT-X) was used to generate 3D topographic images of the cantilever undergoing thermal bending, providing a complete deflection profile along its length. Figure 5 contains an example image insert of a KNT-SThM cantilever

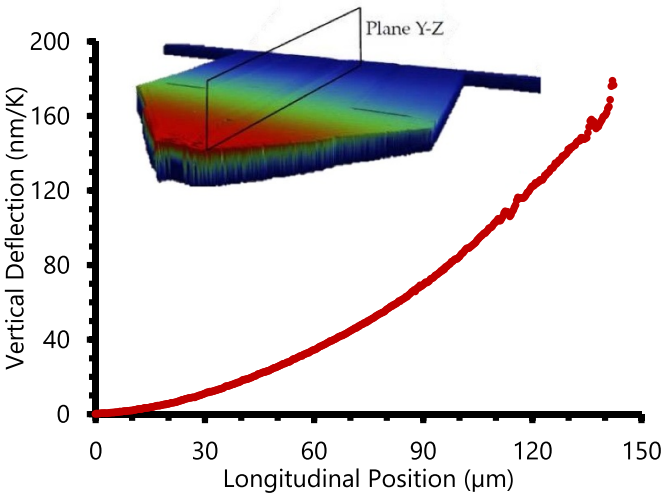

Figure 5. Deflection per kelvin vs. position along a KNT-SThM cantilever undergoing thermal bending using profilometry with example image insert and illustrated *Y*–*Z* plane used for data extraction.

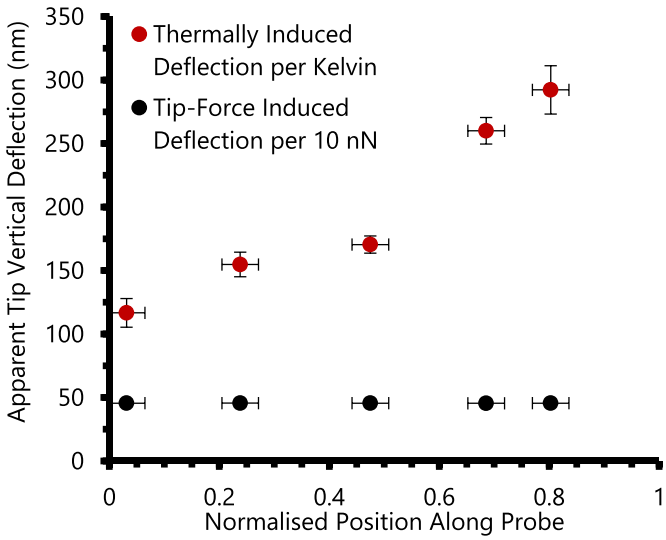

Figure 6. Tip-deflection profiles from a tip-force (10 nN) and thermal bending (per K).

as acquired using the Optical Profilometer. Faint outlines of the underside reflective Au wires can be seen in the image, together with a vertical drop-off at the edge of the probe, both of which are artefacts of the white light interferometry approach, however, neither has a significant impact on the deflection measurement. In the experiment, the SThM probe was positioned less than 1 mm above and parallel to a Peltier Module that induced probe temperature change. Under these conditions, the Peltier is expected to produce a near uniform temperature distribution across and through the probe's cantilever equivalent to an ambient temperature change due the probe's thin nature (550 nm maximum) and low thermal capacity relative to the 40 × 40 mm, 60 W Peltier module. Using this arrangement, two images of the probe, one at ambient, and the second at an elevated temperature were obtained without changing the probe's position. Subtracting the elevated temperature image from the ambient one, allowed the magnitude of KNT-SThM cantilever thermal bending to be determined, as shown in an extracted profile in figure 5. The gradient increase and kink just discernible around 138 μm along the cantilever are due to the probe's tip geometry along with the shaped Au wires and palladium (Pd) tip resistor overlapping as seen in figure 2.

3.2. AFM profile

To understand how thermally induced cantilever bending is interpreted in a normal AFM setup, the Profilometer absolute measurement was compared to the apparent cantilever tip deflection as measured by an optical lever within an AFM instrument. Under the same heat transfer and temperature change, these are expected to demonstrate different profiles due to the AFM applying the tip-force defined InvOLS to the thermally induced rotation at the laser spot. In the experiment, the KNT-SThM probe was mounted into a Digital Instruments Dimension 3100 AFM in the normal manner. The probe was then positioned directly above the Peltier module to impose a similar temperature distribution to that in the Profilometer. As the AFM only extracts a single point measurement through the optical lever, the measurement was repeated for different laser positions along the cantilever. This permitted a profile of cantilever deflection to be generated over five separate points between the cantilever base and tip as limited by the laser spot size (estimated to be a maximum diameter of 60 μm) and location measurement accuracy using the in-built optical microscope. As a further limitation, the SThM tip begins at 139 μm along the cantilever, as seen in figure 2, and no deflection measurements were possible beyond this point. At each laser position, the output of the optical lever was recorded a minimum of five times. In addition, Voltage-distance plots were also obtained for each laser position, allowing the InvOLS at each location to be determined. This allowed the apparent tip-deflection, which is the photodiode output multiplied by InvOLS, to be recorded for each location for both thermally and tip-force induced deflections. The subsequent profile per Kelvin of temperature change is shown in figure 6 together with the profile that 10 nN generates at the same respective points. The tip deflection the latter force generated was based upon a spring constant value of 0.22 N m^{-1} [32], derived from the elastic reference calibration technique which provides a more accurate measurement of SThM cantilever's complex structure [33]. In addition, for this comparison the *x*-axis data was normalised to the total cantilever length (150 μm), permitting later comparison with other AFM cantilevers of different lengths. Uncertainty error-bars in the *x*-data represent the ambiguity of the laser location measurement, while the *y*-uncertainty is the standard deviation of the InvOLS and vertical voltage change from the photodetector (combined through addition of their relative error). For a tip-force, the system outputs a single value as seen in the black data points that is irrelevant of laser position. Regarding the thermal bend profile, an appreciable rotation equal to that seen

with a tip-loaded deflection of around 120 ± 11 nm occurred at the base. This apparent deflection increases towards the tip by approximately two and a half times to a value equivalent to 292 ± 19 nm. What is clear is that, as hypothesised, the Profilometer and AFM profiles are very different with the only similarity being their positive direction. Moreover, the thermally induced deflection is completely different to the tip-force's due to thermal bending having a different relationship between rotation along the cantilever and tip-deflection. It should be highlighted that the deflection of the tip due to a given temperature change is a single value. The error in tip position for a specific temperature change will therefore be a constant, but its interpretation as an additional topographic feature will vary strongly with the longitudinal position of the optical lever laser spot (generally a poorly controlled quantity). To further verify these findings, a comparison to theoretical models was employed.

3.3. Theoretical models

An in-house finite difference method (FDM) model employing superposition of Euler–Bernoulli [34] and thermal bending curvature equations [35] was used to compare cantilever rotation and deflection profiles between tip-force and uniform temperature induced deflection. With the SThM cantilever's Au and silicon nitride construction, the model employed 579 1D elements with a variable element size between 1 µm and 0.025 µm. This allowed for the cantilever geometry to be appreciated, with the finer element applied at the tip where greater dimension change occurs (indicated in figure 7 by the two-coloured regions). It should be noted that the 1D nature of the model meant it provided a single output over the whole cantilever cross-section, an assumption made when applying Euler–Bernoulli beam theory [36]. To ultimately convert the calculated deflection into a value equivalent to that recorded by the AFM, a theoretical InvOLS was required. This was determined for each 'virtual laser position' by taking tip-deflection in the model and dividing it by the rotations (equivalent to photodetector vertical voltage) at each location along the cantilever. By taking these theoretical sensitivities and applying them to the modelled cantilever behaviour, the data could be presented in a format equivalent to that obtained during the AFM experiment of figure 6. This is shown in figure 7 using the same units as those output by the experiment. It can be seen from these figures that both modelled and experimental data for thermal induced deflection show a similar trend of an initial deflection at the cantilever base that increases gradually until half-way where it increases at a greater rate towards the tip. Although this is not a perfect match due to the limited number of data points in the experiment, it shows a similar trend and magnitude that strongly indicates that they are demonstrating the same phenomenon. Unsurprisingly, other bi-material AFM cantilevers exhibit the same variation with change in the optical lever laser's location. This was verified through repeat experiments using MLCT-B, MLCT-C [37] and PNP-DB [38] cantilevers elsewhere [32]. In summary, out-of-contact thermal bending is widely variable and inherently misinterpreted in the AFM's outputs. This is due to an inability to distinguish between tip-force and thermally induced deflection, resulting in the control loop responding to both identically resulting in incorrect control of the cantilever.

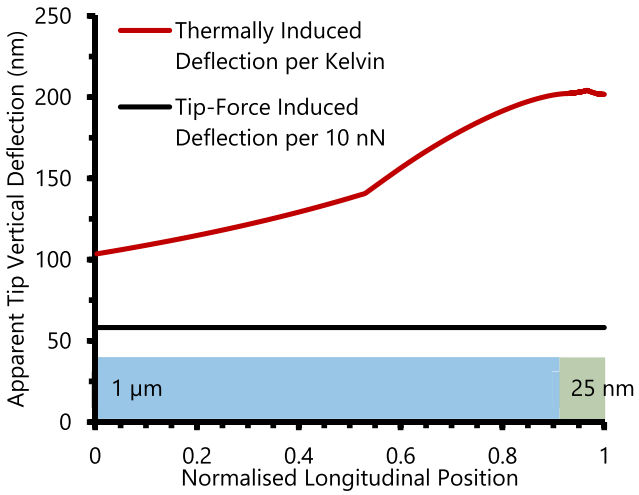

Figure 7. FDM—thermal bend & tip-force induced deflection profiles using theoretical InvOLS with coloured regions indicating model's mesh technique.

4. Measuring in-contact thermal bending

The above results clearly demonstrate AFM's behaviour for cantilever thermally bending when out-of-contact. However, it is essential to also consider the case when the cantilever tip is in-contact with the sample surface (as is the case during contact-mode scanning). In this case, an array of forces interact with the tip of the cantilever, such as van der Waals, Capillary, Coulomb and Pauli-exclusion [39]. This results in the tip being mechanically linked to the surface, leading to different boundary conditions when compared to the out-of-contact situation considered above. This was explored once again by employing KNT-SThM probes within a Dimension 3100 AFM.

4.1. Experimentation

To obtain the in-contact thermal deflection profiles, a microscopic, isolated heater was required to minimise temperature induced sample expansion. This ensured that cantilever thermal bending generated the majority of any thermal deflection measured by the AFM. A microheater described by Dobson *et al* (figure 8) [40] provided a suitable device. Characterisation of this demonstrated that the heated region on the device was limited to the area of the membrane. Therefore, positioning the tip over the main silicon-backed chip immediate to the membrane, with the cantilever located above the heater and membrane (figure 9), resulted in cantilever heating without mechanical displacement of the tip. It should be noted that this microheater resulted in a less uniform temperature distribution across the cantilever length when compared to the Peltier heater utilised previously. To account for

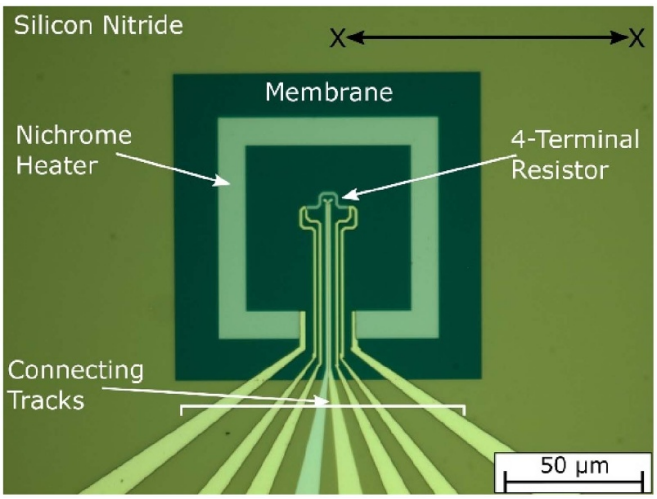

Figure 8. Optical image of employed microheater.

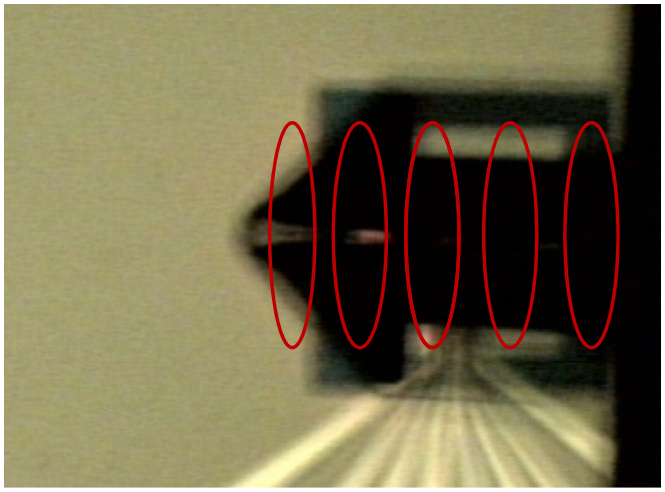

Figure 9. Image of KNT-SThM probe over the microheater through the AFM optical microscope with laser locations indicated in red.

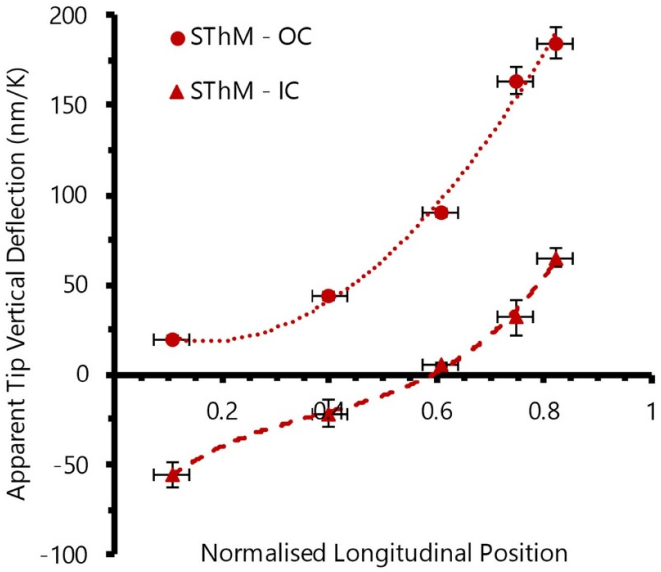

Figure 10. Out-of-contact (OC) & in-contact (IC) thermal bend deflection profiles of a KNT-SThM cantilever.

this, out-of-contact cantilever thermal bend was also measured using the microheater with the tip withdrawn vertically a short distance (less than 1 µm) out-of-contact. With these operating conditions established, the laser was positioned at five different longitudinal locations (shown in figure 9) and both the InvOLS and deflection-temperature gradients were measured in the same manner as described in the previous Peltier AFM experiment. The results for both the out-of-contact and in-contact deflection profiles can be seen in figure 10. In this plot, the *y*-axis has been normalised using the temperature measured by the SThM with *x* and *y*-errors determined in the same manner as in figure 6. A third-order polynomial trendline has been imposed to help guide the eye between the points. Analysing the out-of-contact profile, the measured deflection tends towards zero at the cantilever base, increasing as the laser is positioned further along the cantilever. This can be explained by the non-uniform cantilever temperature distribution due to the microheater leaving the probe's silicon chip unheated so that the cantilever base constitutes a constant thermal boundary at (or close to) ambient temperature. With the silicon AFM probe chip acting as a heat sink, it is understandable that the cantilever base experienced a greatly reduced temperature change and subsequent deflection when compared to the Peltier experiment in figure 6. However, repeating the measurement with the probe tip in-contact with the microheater substrate resulted in a markedly different profile as shown in figure 10. At the base of the cantilever, a negative deflection was measured. It increased to zero around mid-way along the cantilever, after which point the measured tip-deflection became positive towards the tip. This is significantly different to the out-of-contact measurement and strongly suggests a different manifestation of thermal bending. When considering these results, it is essential to remember that although the microscope outputs a signal labelled 'tip-deflection', the AFM system in fact is directly measuring change in cantilever rotation through the photodetector's vertical voltage. Subsequent application of the relevant InvOLS to this then provides the tip-deflection interpretation. Therefore, to further visualise the true cantilever deflection, as well as investigate how the tip contact boundary condition changed thermal bending, a theoretical model was employed.

4.2. Theoretical model

In section 3.3 a FDM model was utilised that assumed a 1D cantilever structure. However, due to the greater complexity of tip contact, finite element analysis (FEA) was employed. This made use of the same geometry and material properties as the FDM model with different tip-sample contact boundary conditions. Prior to constructing this model, the most appropriate tip boundary condition needed to be established. Fixed and Roller contacts were both considered due to the presence of static and kinetic friction at the tip-sample contact. The former produces zero tip movement, while the latter permits horizontal

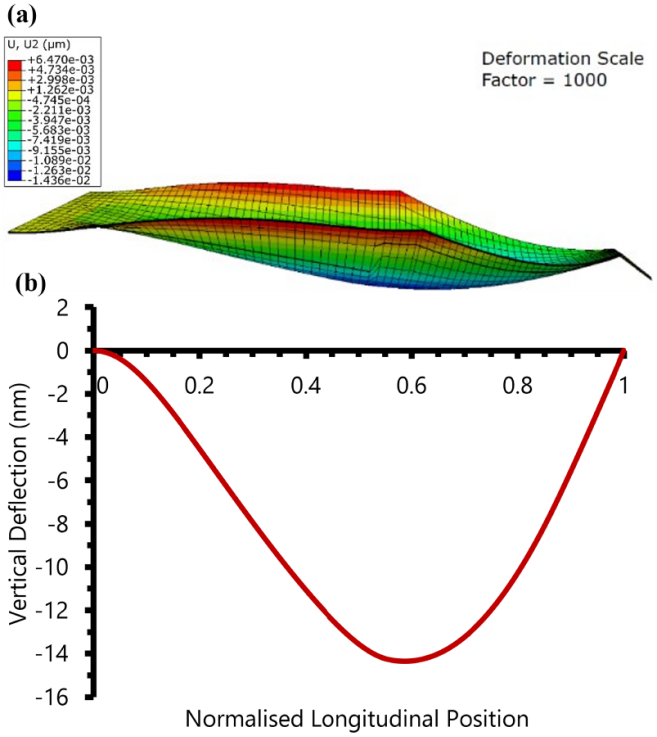

Figure 11. FEA model of a KNT-SThM cantilever with a Roller tip contact undergoing 1 K temperature change in (a) 3D view; (b) centreline profile.

movement with resistance. In reality, either Fixed or Roller scenarios are plausible depending upon the magnitude of the frictional force at the tip, with factors such as tip-normal-force, environmental conditions, sample material and contact area all playing a role [41]. Quantification of the coefficient of friction was performed for the specific KNT-SThM tip utilised in this paper against a polished silicon surface. This employed the tilted reflective surface and lateral friction loop technique described by Munz [42] and generated a coefficient of friction of 0.208 ± 0.13. This employed five different normal tip forces, and theoretical normal and torsional spring constants from FEA were employed with the experimental data to determine the coefficient of friction. Hence, a 50 nN vertical force (including adhesion force) was found to generate 10 ± 7 nN of frictional force due to the experimentally determined coefficient that links them. This is relatively low and a change of only a tenth of a Kelvin would theoretically generate enough longitudinal force to overcome this. Lateral friction cannot be equal to longitudinal due tip asymmetry, but assuming it is not significantly different, the tip will still displace horizontally for low temperature changes. Hence, a Roller was selected as the most appropriate tip boundary condition when scanning smooth samples such as silicon. The FEA output can be seen for thermal bending with no applied friction in figure 11. This is significantly different to that produced when the cantilever was out-of-contact, as seen in figure 5. This theoretical result aligns well with experimental observations in figure 10, with the change in gradient seen in the model's profile matching the deflection direction of the AFM from negative to positive further along the cantilever. This demonstrates and confirms that the tip boundary condition imposed by tip-surface contact causes a complete change in how cantilever thermal bending manifests. Moreover, it would be expected that this in-contact thermal bending phenomenon would occur when in vacuum, gas, or liquid as it is dictated by the cantilever's tip-contact. However, variations in heat transfer, cantilever temperature distribution and tip-sample stiction in each environment may alter the exact form and adhesion limits. With this said and agreement between experiment and model, one important observation that can be made from the profile shown in figure 11, is the point of zero rotation present mid-way along the thermally deflected cantilever. This additionally occurs in the experimental data shown in figure 10, whereby zero rotation would correspond to zero apparent tip deflection. As a result, it offers the possibility that if the optical lever laser spot is positioned at this location, zero thermal induced deflection will be interpreted.

5. Quantification of in-contact thermal bending in non-thermal AFM cantilevers

To further explore the observations above, in-contact deflection profiles were obtained using a range of AFM probes employing the same microheater experiment described previously. These had a similar material composition of silicon nitride and Au to the SThM probes with key nominal values stated in table 1 and optical images of each shown in figure 12. Alongside these probes, a reference cantilever consisting of an Uncoated-SThM (UC-SThM) cantilever was included. This was a standard KNT-SThM probe from which all the Au metal had been etched away, leaving a silicon nitride cantilever. Consequently, the spring constant and resonant frequency will deviate from the nominal values quoted in table 1. The respective AFM tip-deflection profiles are shown in figure 13, with the deflection normalised to cantilever temperature, as measured using a KNT-SThM probe. The same error determination method described previously was employed to generate errorbars.

All the probe cantilevers exhibited an opposite deflection direction to the KNT-SThM probes. This was expected since their metallisation is on the opposite side of the cantilever. What is additionally clear from the figure 13 is that although the temperature distributions and geometries differed between the cantilevers, the location of their deflection turning point appeared consistently between 0.55 and 0.6 (55% and 60%) along each cantilever. This is a very similar location to that observed for the KNT-SThM cantilever. This is reasonable, as it is expected that thermal bending is strongly and consistently dictated by the tip's boundary condition. As with most AFM cantilevers, those used in this study had a relatively uniform cross-section along most of their length. This, with the near-identical surface contact conditions, resulted in a turning point occurring at a consistent location along the cantilevers. This suggests that when using an optical lever measurement of in-contact cantilever deflection, there is an opportunity to eliminate cantilever thermal bending artefacts in topographic

Table 1. Manufacturer nominal values for non-thermal AFM cantilevers employed [26, 37, 38].

Probe	Length × width × thickness (μm)	Spring constant (N m^{-1})	Resonance frequency (kHz)
MLCT-B	210 × 20 × 0.55	0.02	15
MLCT-C	310 × 20 × 0.55	0.01	7
PNP-DB	100 × 40 × 0.6	0.48	67
UC-SThM	150 × 120 × 0.4	0.5	50

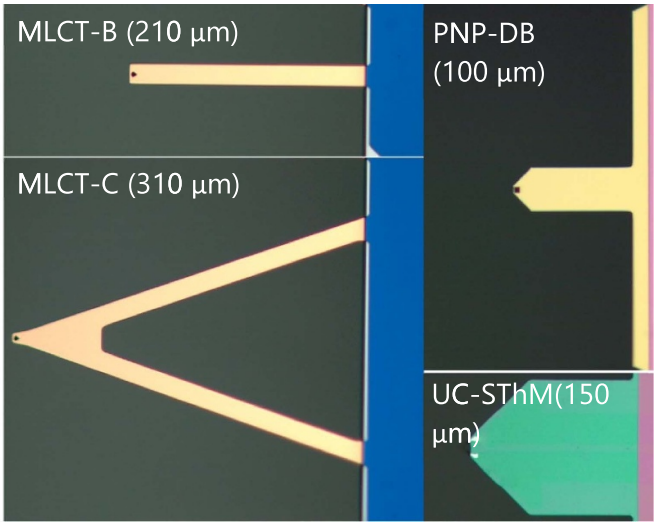

Figure 12. Optical images of non-thermal AFM cantilevers with their nominal lengths indicated.

imaging by careful positioning of the laser spot towards the centre of the cantilever's length. It should be noted that reflecting the laser at this position will result in a reduced force-deflection signal when compared to locating the laser reflection at the cantilever tip, as is the convention, but the reduced sensitivity is well compensated by a potentially enormous increase in accuracy of measurement.

Based upon the results and analysis above, all multi-material probe cantilevers will produce this in-contact behaviour of zero optical lever measured thermal bend deflection near mid-way along the cantilever. This location may alter slightly with non-uniform temperature distributions or cantilever shapes, but has been found to be relatively robust from 55% to 60% along their lengths based upon the different cantilever shapes and variable temperature distributions they experienced in this work.

6. AFM scans

The above conclusions can be extended to investigate the impact of thermal bending on contact mode topographic scans. To visualise the impact of this phenomenon on topographic images, contact AFM scans were performed over heated and unheated regions of the microheater already described. Initially, single line scans were used to explicitly quantify topographic deviation due to in-contact thermal bending.

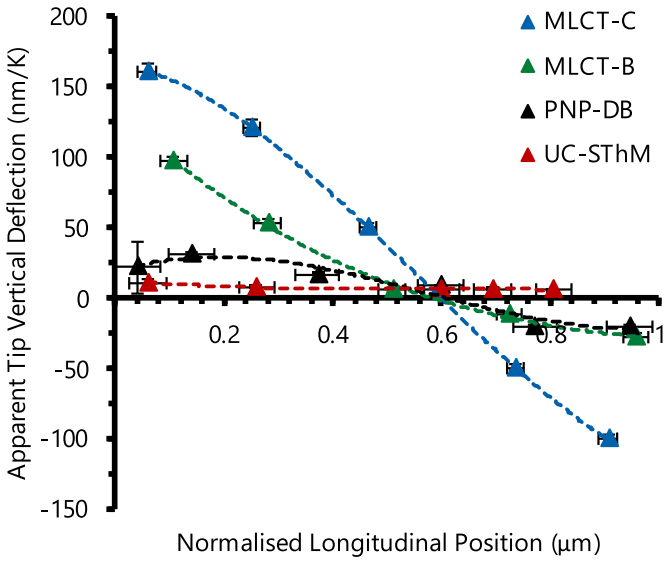

Figure 13. In-contact thermal bend profiles for AFM cantilevers.

Following this, full scans of the microheater were employed to provide a more complete perspective.

6.1. Line scans

Scans were taken along the *X*–*X* line shown in figure 8. This resulted in the cantilever overlapping both the microheater and surrounding unheated silicon nitride at different points in the scan. The scans were repeated for three different laser positions at the tip, base and middle: approximately 100%, 20% and 60% along the cantilever respectively. This allowed the three key laser reflection regions seen in the stationary experiments of negative, positive and near zero change to be demonstrated. KNT-SThM and MLCT-B probes where utilised, with the SThM probe providing simultaneous topography and tip temperature, but the MLCT-B probe only measuring topography. A subtraction of the unpowered microheater from the powered one for each laser position is shown in figures 14 and 15 with no plane-fitting applied.

From figure 14(a), the temperature changes measured at each laser position are very similar with a maximum change of 2 K along the scan. With such similar temperature scans and a flat sample, the variation in measured topography is quite striking. The change in measured topography between the base and tip laser location outputs are completely opposite, with a topographic range of 150 nm and −170 nm respectively. The middle laser reflection exhibited much lower variation in topography even though the scan encompassed the same temperature conditions and scan region. Regarding the MLCT-B scan shown in figure 15, a similar trend can be seen where the deflection directions are opposite (as explained previously). A topography range of 373 nm and −237 nm is seen over the microheater for the cantilever base and tip locations respectively. Additionally, the middle laser location displayed only 11 nm topographic variation scanning between the unheated and heated regions (a 97% reduction relative to the base laser position scan range). Overall, these are in strong

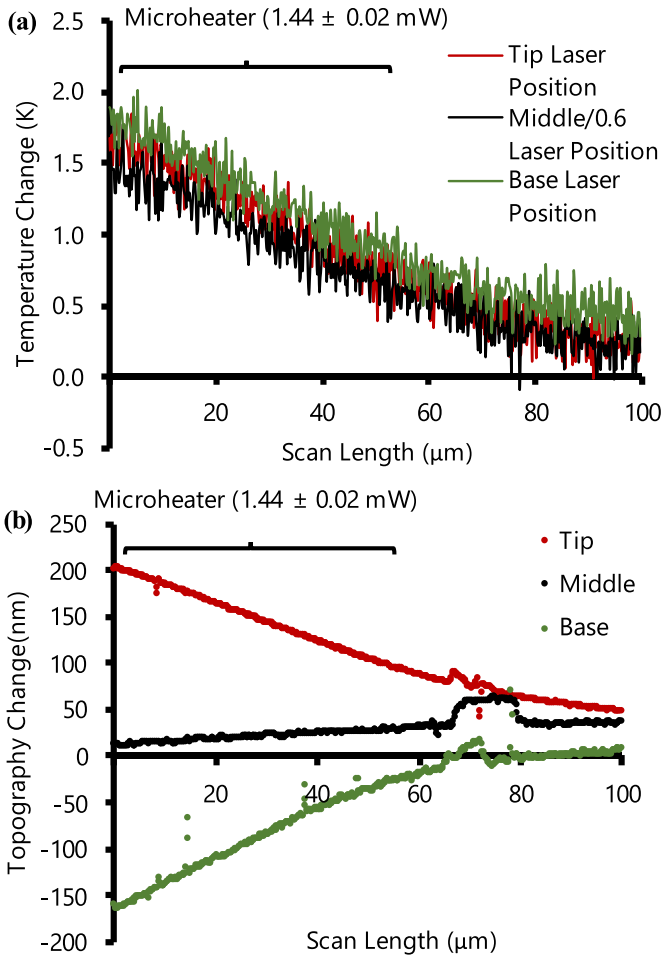

Figure 14. SThM line scans of (a) temperature change; (b) topography change.

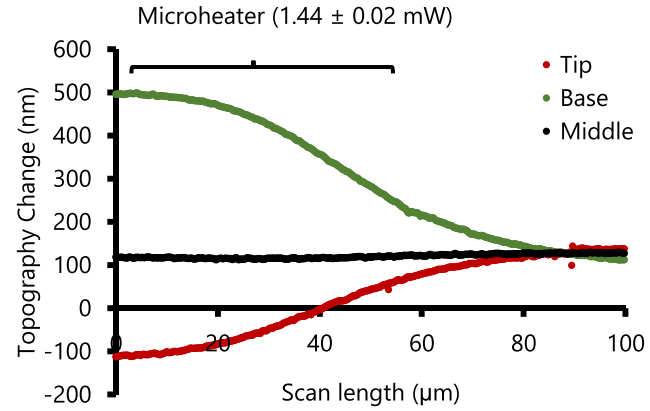

Figure 15. MLCT-B line scans of topography change.

agreement with the previous static experiments, demonstrating the large variation in topographic measurement that can occur under modest temperature variations. Moreover, for all laser locations, this manifests in the feedback loop generating an erroneous tip-force compared to the desired magnitude for

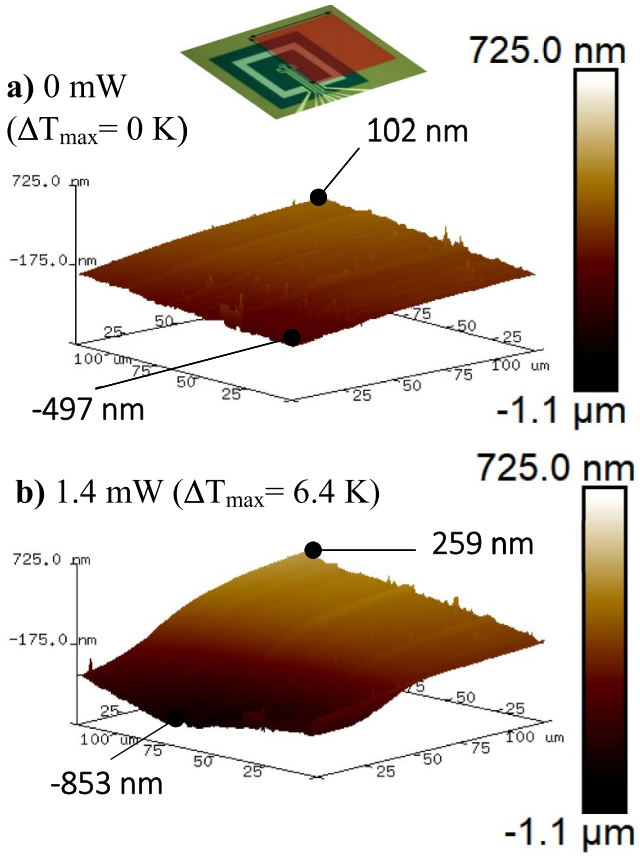

Figure 16. Full MLCT-B AFM scan—tip laser spot of (a) unpowered; (b) powered microheater with graphic depiction of scanned area (top).

the scan. This adds another variable and inconsistent component to the interpretation of topographic images, especially on softer materials.

6.2. *Full scans*

Utilising the same *X*–*X* line shown in figure 8 as the first line of a square scan extending down the right-side of the microheater, full AFM scans were generated (as demonstrated by the red box in the graphic insert in figure 16). This was carried out using only the MLCT-B probe as the KNT-SThM probes would form an electrical connection with the microheater during scanning, resulting in inaccurate temperature measurement and potentially destroying the thermal sensor or microheater. The MLCT-B probe was scanned in the same region over the unpowered and powered microheater, using similar laser positions to the line scans (tip, base and middle). As the scan was performed over the microheater, a quantification of power vs membrane thermal deflection was performed using the Profilometer, ascertaining that for 1.4 mW, the membrane displaces by −7 nm at its centre. Hence, AFM measured displacement out-width this will be due to the cantilever thermally bending. Data pairs (unpowered and powered microheater) for each laser position are presented with the same Z-scale in figures 16–18 to allow clear comparison (the scan area being the red box in figure 16's graphic insert). The maximum

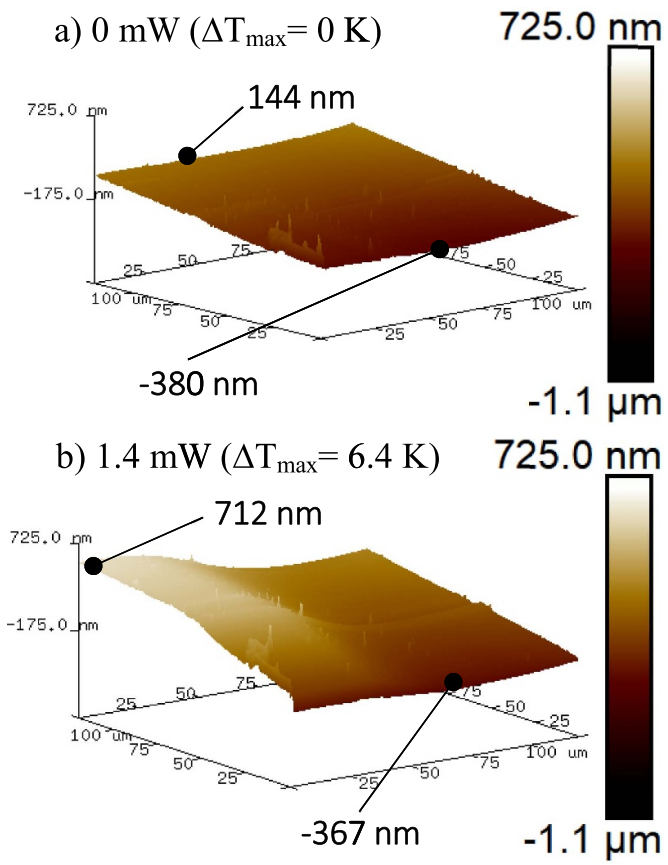

Figure 17. Full MLCT-B AFM scan—base laser spot of (a) unpowered; (b) powered microheater.

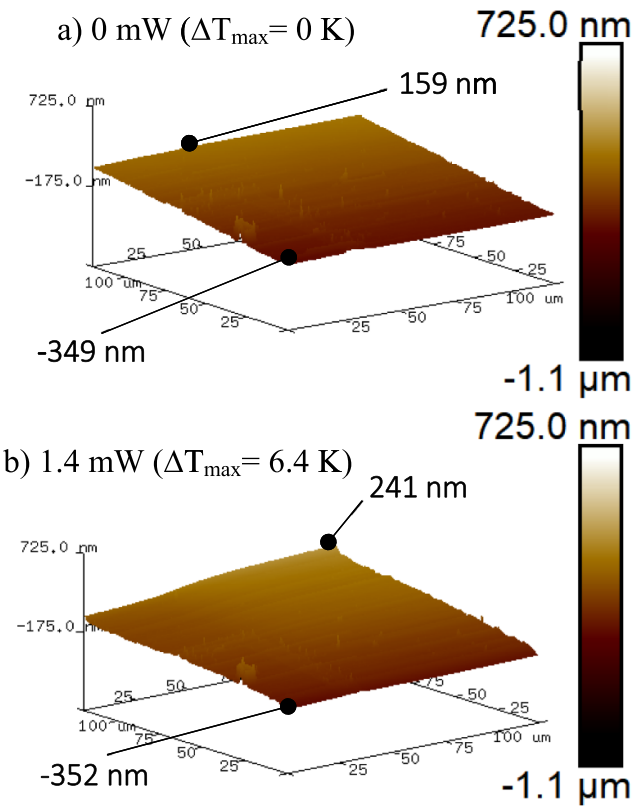

Figure 18. Full MLCT-B AFM scan—middle laser spot of (a) unpowered; (b) powered microheater.

and minimum topographic measurements are highlighted for clarity.

In these scans, the microheater appears as a negative topographic feature when the optical lever's laser was positioned at the tip of the cantilever (figure 16) and a positive feature when the laser was positioned at the base (figure 17). The scan obtained with the laser reflected from the middle of the cantilever shows relatively little topographic change in comparison (figure 18). Although vastly reduced in comparison to the base and tip laser positions, a dip still occurred on the left over the microheater. This will be a combination of the microheater displacing (although low according to the Profilometer measurements previously mentioned), variable temperature distribution along the cantilever, slightly imperfect laser position and extent of the laser spot. Overall, these scans clearly demonstrate that optical lever laser positioning has a pronounced and variable effect on AFM topographic measurement in thermally variable environments, but that relative thermal insensitivity is possible through laser positioning at 60% along bimetallic probes. However, it should be noted that the commonly used thermal noise method for spring constant calibration is sensitive to laser positioning away from the cantilever free-end [43]. Therefore, any calibration using this approach should be performed prior to re-positioning the laser 60% along the cantilever. In addition, it should also be remembered that too low a contact force during scanning will render the scan more susceptibility to contact loss from temperature changes due to less attractive forces to overcome. As a result, for consistent scans and execution of the 60% laser re-positioning strategy, this force needs to be large enough to maintain contact for the temperature change experienced alongside appropriate feedback coefficients.

7. Conclusion

Overall, bimaterial/bimetallic bending can be a major contributor to thermal drift in AFM images acquired using multi-material cantilevers. Its manifestation can be clearly seen, but relating AFM measured deflection to thermal bending is non-trivial due to the ubiquitous use of the optical lever detection method. Out-of-contact and in-contact scan regimes demonstrate starkly different thermal bending behaviours due to their differing tip boundary conditions. The former produces significant, single-direction cantilever deflection, while the latter generates a more complex deflection profile that can result in contact-mode topography artefacts in either the positive or negative direction depending on laser position. These thermally induced artefacts are indistinguishable from topographic signals unless extreme care is taken by measuring the sample over a range of temperatures to observe thermally induced variations. However, for all multi-material AFM probes tested in this work, in-contact cantilever deflections always exhibit a turning point located between 55% and 60% along their length. Therefore, positioning the reflected

optical lever laser spot at this region produces measurements that are largely insensitive to thermal bending. The exact location of this turning point appears reasonably robust, although not perfectly consistent, depending on cantilever geometry, material and temperature distributions. By employing this approach, a 97% reduction in thermal topographic artefacts was demonstrated simply through laser positioning in an otherwise unmodified AFM.

Data availability statement

All data that support the findings of this study are included within the article (and any supplementary files).

Acknowledgments

The authors thank the Engineering and Physical Sciences Research Council (EPSRC) for funding this work and the James Watt Nanofabrication Centre at the University of Glasgow for the provision of experimental facilities.

ORCID iDs

Christopher W Mordue https://orcid.org/0000-0003-0819-7285
Phillip S Dobson https://orcid.org/0000-0001-5137-8298

References

[1] Binnig G and Quate C F 1986 Atomic force microscope *Phys. Rev. Lett.* **56** 930–3
[2] Jalili N and Laxminarayana K 2004 A review of atomic force microscopy imaging systems: application to molecular metrology and biological sciences *Mechatronics* **14** 907–45
[3] Meyer G and Amer N M 1988 Novel optical approach to atomic force microscopy *Appl. Phys. Lett.* **53** 1045–7
[4] Putman C A J, De Grooth B G, Van Hulst N F and Greve J 1992 A detailed analysis of the optical beam deflection technique for use in atomic force microscopy *J. Appl. Phys.* **72** 6–12
[5] Woodward J T 1998 Removing drift from scanning probe microscope images of periodic samples *J. Vac. Sci. Technol.* B **16** 51
[6] Radmacher M, Cleveland J P and Hansma P K 1995 Improvement of thermally induced bending of cantilevers used for atomic force microscopy *Scanning* **17** 117–21
[7] Marinello F, Balcon M, Schiavuta P, Carmignato S and Savio E 2011 Thermal drift study on different commercial scanning probe microscopes during the initial warming-up phase *Meas. Sci. Technol.* **22** 1–8
[8] Te Riet J *et al* 2011 Interlaboratory round robin on cantilever calibration for AFM force spectroscopy *Ultramicroscopy* **111** 1659–69
[9] Wenzler L A, Moyes G L and Beebe T P 1996 Improvements to atomic force microscopy cantilevers for increased stability *Rev. Sci. Instrum.* **67** 4191–7
[10] Wang T, Ma C, Chen Y, Chu J and Huang W 2015 Effects of temperature and humidity on atomic force microscopy dimensional measurement *Microsc. Res. Tech.* **78** 562–8
[11] Schumacher Z, Miyahara Y, Aeschimann L and Grütter P 2015 Improved atomic force microscopy cantilever performance by partial reflective coating *Beilstein J. Nanotechnol.* **6** 1450–6
[12] Méndez-Vilas A, González-Martín M L and Nuevo M J 2002 Optical interference artifacts in contact atomic force microscopy images *Ultramicroscopy* **92** 243–50
[13] Mertens J, Finot E, Thundat T, Fabre A, Nadal M-H, Eyraud V and Bourillot E 2003 Effects of temperature and pressure on microcantilever resonance response *Ultramicroscopy* **97** 119–26
[14] Murrell M P, Welland M E, O'Shea S J, Wong T M H, Barnes J R, McKinnon A W, Heyns M and Verhaverbeke S 1993 Spatially resolved electrical measurements of SiO_2 gate oxides using atomic force microscopy *Appl. Phys. Lett.* **62** 786–8
[15] Nonnenmacher M, O'Boyle M P and Wickramasinghe H K 1991 Kelvin probe force microscopy *Appl. Phys. Lett.* **58** 2921–3
[16] Martin Y and Wickramasinghe H K 1987 Magnetic imaging by 'force microscopy' with 1000 Å resolution *Appl. Phys. Lett.* **50** 1455–7
[17] Pylkki R, Moyer P and West P 1994 Scanning near-field optical microscopy and scanning thermal microscopy *Jpn. J. Appl. Phys.* **33** 3785–90
[18] Sevim S, Tolunay S and Torun H 2015 Micromachined sample stages to reduce thermal drift in atomic force microscopy *Microsyst. Technol.* **21** 1559–66
[19] Marinello F, Bariani P, De Chiffre L and Savio E 2007 Fast technique for AFM vertical drift compensation *Meas. Sci. Technol.* **18** 689–96
[20] Zhang T, Zhao Y, Tong Z and Guan Y 2016 A novel method to calculate the mechanical properties of cancer cells based on atomic force microscopy *Acta Bioeng. Biomech.* **18** 19–24
[21] D'Acunto M and Salvetti O 2011 Pattern recognition methods for thermal drift correction in atomic force microscopy imaging *Pattern Recognit. Image Anal.* **21** 9–19
[22] Krauskopf J E, Bartenwerfer M and Fatikow S 2016 Modeling and compensating thermal drift in time divergent AFM measurements *Micro-Nano-Integration; 6. GMM-Workshop* pp 1–6
[23] Shekhawat G S, Chand A, Sharma S, Verawati V and Dravid P 2009 High resolution atomic force microscopy imaging of molecular self assembly in liquids using thermal drift corrected cantilevers *Appl. Phys. Lett.* **95** 233114
[24] Beyder A, Spagnoli C and Sachs F 2006 Reducing probe dependent drift in atomic force microscope with symmetrically supported torsion levers *Rev. Sci. Instrum.* **77** 056105
[25] Slattery A D, Blanch A J, Quinton J S and Gibson C T 2013 Calibration of atomic force microscope cantilevers using standard and inverted static methods assisted by FIB-milled spatial markers *Nanotechnology* **24** 015710
[26] Bruker 2021 *VITA—SThM* (available at: www.brukerafmprobes.com/c-205-vita-sthm.aspx) (Accessed 2 July 2023)
[27] Sander M 1993 A multipurpose scanning probe microscope *Rev. Sci. Instrum.* **64** 2591–4
[28] Hutter J L 2005 Comment on tilt of atomic force microscopy cantilevers: effect on spring constant and adhesion measurements *Langmuir* **21** 2630–2
[29] Costa N P D and Hoh J H 1995 Calibration of optical lever sensitivity for atomic force microscopy *Rev. Sci. Instrum.* **66** 5096–7
[30] Ge Y 2016 Quantitative measurement using scanning thermal microscopy *PhD Thesis* University of Glasgow
[31] Zhang Y, Dobson P S and Weaver J M R 2012 High temperature imaging using a thermally compensated cantilever resistive probe for scanning thermal microscopy *J. Vac. Sci. Technol.* B **30** 1–5

[32] Mordue C 2022 Modelling, quantifying and attenuating multi-material thermal bend in atomic force microscopy cantilevers *PhD Thesis* University of Glasgow
[33] Avilovas L 2021 Micro electro-mechanical system design, fabrication and application for atomic force microscopy probe elasticity characterisation *PhD Thesis* University of Glasgow
[34] Gere J M 2004 *Mechanics of Materials* 6th edn (Thomson Learning Inc)
[35] Hsueh C H 2002 Modeling of elastic deformation of multilayers due to residual stresses and external bending *J. Appl. Phys.* **91** 9652–6
[36] Oñate E 2013 *Structural Analysis with the Finite Element Method Linear Statics* vol 2, 1st edn (Springer)
[37] Bruker 2023 *MLCT* (Bruker) (available at: www.brukerafmprobes.com/p-3444-mlct.aspx) (Accessed 23 June 2023)
[38] Nanoworld Innovative Technlogies 2023 Nanoworld ® SPM and AFM probes
[39] Bhushan B 2005 *Nanotribology and Nanomechanics* 1st edn (Springer)
[40] Dobson P S, Mills G and Weaver J M R 2005 Microfabricated temperature standard based on Johnson noise measurement for the calibration of micro- and nano-thermometers *Rev. Sci. Instrum.* **76** 054901
[41] Wang Y and Wang J 2018 Friction determination by atomic force microscopy in field of biochemical science *Micromachines* **9** 18–20
[42] Munz M 2010 Force calibration in lateral force microscopy: a review of the experimental methods *J. Phys. D: Appl. Phys.* **43** 063001
[43] Sader J E, Lu J and Mulvaney P 2014 Effect of cantilever geometry on the optical lever sensitivities and thermal noise method of the atomic force microscope *Rev. Sci. Instrum.* **85** 113702